Università degli Studi di Napoli "Federico II"

SCUOLA POLITECNICA E DELLE SCIENZE DI BASE

DIPARTIMENTO DI INGEGNERIA INDUSTRIALE

CORSO DI LAUREA IN INGEGNERIA AEROSPAZIALE

CLASSE DELLE LAUREE IN INGEGNERIA INDUSTRIALE (L-9)

Elaborato di laurea in Meccanica del Volo

Geometric modelling, stability and control analysis of the unmanned aerial vehicle Bayraktar TB-2 with OpenVSP

Relatore:
Prof. Danilo Ciliberti

Candidato:
Yasmine Marotta
Matr. N35003525

ANNO ACCADEMICO 2021 – 2022

À mes grandparents, Hamidou et Mouima

Abstract

The purpose of the following work is to perform an analysis and the modelling of the Bayraktar TB-2 unmanned aerial vehicle using OpenVSP, an open-source parametric tool for aircraft geometry, which can be used to construct 3D aircraft models and to aid in engineering analysis of those models. Stability and control analysis can be done on the geometric model using one of the tools provided by the software, specifically the VSPAERO tool, a fast, linear, lattice-based vortex solver. Assuming the simulation is appropriately set up and the model properly constructed, the program generates valid and reliable results. In this scenario, the software appeared to be both rapid and convenient, from the geometric design through data analysis. The Vortex lattice method was chosen as the numerical method for aircraft aerodynamic analysis in this thesis study. The data was then compiled and commented in order to depict a comprehensive scenario involving static stability and control. The lifting surfaces are modelled by equating them to an infinitely thin sheet of discrete vortices. Although the tool has its limitations for more complex models, it has been proven to be a reasonable solution for simple designs that require simple preliminary numerical analysis.

Sommario

Lo scopo del seguente lavoro è quello di effettuare una analisi e la modellazione del velivolo unmanned Bayraktar TB-2, adoperando OpenVSP, uno strumento parametrico open source per il design di geometrie di velivoli che può essere usato per costruire modelli 3D di velivoli e come aiuto per l'analisi ingegneristica degli stessi. L'analisi di stabilità e controllo sul modello geometrico può essere eseguita servendosi di uno degli strumenti forniti dal programma, in particolare VSPAERO, un solutore veloce, lineare e basato su reticoli di vortici. Supponendo che la simulazione è stata adeguatamente configurata e il modello realizzato correttamente, il programma genera risultati validi e attendibili. In tal caso, il software si è rivelato essere veloce e conveniente, dal design del modello geometrico all'analisi dei dati. È stato scelto, per ottenere i risultati presenti in questa tesi, come metodo numerico il Vortex Lattice Method. I dati sono stati poi raccolti e commentati al fine di dipingere un quadro completo su stabilità e controllo. Le superfici portanti sono state modellate come lastre infinitamente sottili di vortici discreti. Nonostante i suoi limiti per modelli più complessi, lo strumento si è dimostrato essere una soluzione conveniente per design semplici che necessitano di una semplice analisi numerica preliminare.

Table of contents

List of figures

List of tables

1. Introduction

1.1 Objective

The objective of this work is to completely portray the aerodynamic and stability analysis of the unmanned aerial vehicle Bayraktar TB-2. The findings obtained from this study are a preliminary data set, as both VSPAERO and the Vortex Lattice Method present their limits, therefore they can only be used as a first evaluation of aerodynamic performance, stability and control. Moreover, the thesis aims to clarify the VLM numerical method, its fundamental theory and how it is implemented by the software used. The under-analysis UAV's characteristic curves and other valuable data, such as the lift, aerodynamic efficiency, moment coefficient and drag polar curves for the isolated wing, partial and complete aircraft, were obtained via Microsoft Excel data processing. Lastly, aircraft stability observations are also made considering a table generated by starting the analysis at a set angle of attack.

1.2 Layout of the work

Chapter 1: In this chapter a brief introduction on the vehicle is made as well as presenting the basics UAV information.

Chapter 2: This chapter illustrates the core assumptions behind the Vortex lattice method and its consequences.

Chapter 3: In this chapter the OpenVSP software will be presented along with the tools used for this work as well as illustrating how the model has been created.

Chapter 4: In this final chapter the results are presented and analysed in order to deduce information regarding the stability and control of the vehicle.

1.3 Bayraktar TB-2

1.3.1 Bayraktar TB-2

The Bayraktar TB-2 is a Turkish unmanned tactical armed UAV system, developed and manufactured by Baykar. A highly sophisticated design that provides all solutions required by the operator in a single integrated system. The UAV in question is a Medium Altitude Long Endurance vehicle (MALE), capable of conducting intelligence, surveillance and reconnaissance (ISR) and armed attack missions, using the four guided missiles carried beneath the wings. In challenging and meteorological and geographical conditions, such as high temperatures and sandstorms, the Bayraktar TB-2 holds the Turkish aviation record for endurance and altitude, with 27 hours 3 minutes and 25030 feet.

Figure 1.1.1 The Bayraktar TB-2.

The system consists in an armed platform, a Ground Control Station, a Ground Data Terminal, a Remote Display Terminal, an Advanced Base equipped with a generator and trailer modules.

The aircraft distinguishing feature is its tail plane, which is an inverted V-tail, where the movable control surfaces are known as ruddervators, functioning as rudders when moving differentially and as elevators when moving together. This UAV is also equipped with other control surface.

The structure presents a twin boom arrangement in addition to the engine installed as a pusher system just aft of the wing, as this configuration unburdens the front of the fuselage from payload installation while protecting the engine and the propeller, besides providing an unobstructed view forward. The induced air velocity, caused by using a propeller in this configuration, does not increase the fuselage friction drag compared to the slipstream in a front-mounted tractor propeller configuration.

1.3.2 UAV flight stability and stability derivatives

Stability is defined as the tendency of the UAV to return to a condition of equilibrium when subjected to a disturbance in flight, typically caused by gusts or flight control input. Specifically static stability, which can be positive, negative, divergent or neutral, is the initial response of the aircraft to regain equilibrium upon a disturbance. [1]

The Neutral Point (NP) is the location of the aircraft's centre of gravity (CG) that would result in neutral static longitudinal stability.

The stability criterion is expressed in terms of the aircraft's static margin (SM), which is the distance between the CG and the NP in body axes and defined as a non-dimensional measure of the aircraft's stability, since the longitudinal stability heavily depends on the CG's location. It is neutral when the CG is located at the aircraft's neutral point, positive when positioned ahead of the NP, and negative when moved aft.

A high SM denotes a fairly stable but not particularly manoeuvrable aircraft, while UAV with high manoeuvrability have a low, positive SM. Consequently, the CG must be in front of the NP in order to obtain positive static longitudinal stability.

During flight, moments on a UAV are created by the aerodynamic load distribution and the thrust force not acting through the CG. Aerodynamic moments are expressed in terms of the dimensionless coefficients for pitching moment (Cm), rolling moment (Cℓ) and yawing moment (Cn). The values of Cm, Cℓ and Cn depend on the angle of attack (α), Reynolds number (Re), Mach number (M) and sideslip angle (β) and are functions of the angular rates and sideslip of the aircraft. A necessary condition for longitudinal static stability of the UAV is that the pitching moment curve has a negative slope through the equilibrium point. The slope must be negative for lateral static stability and positive for directional static stability. [1]

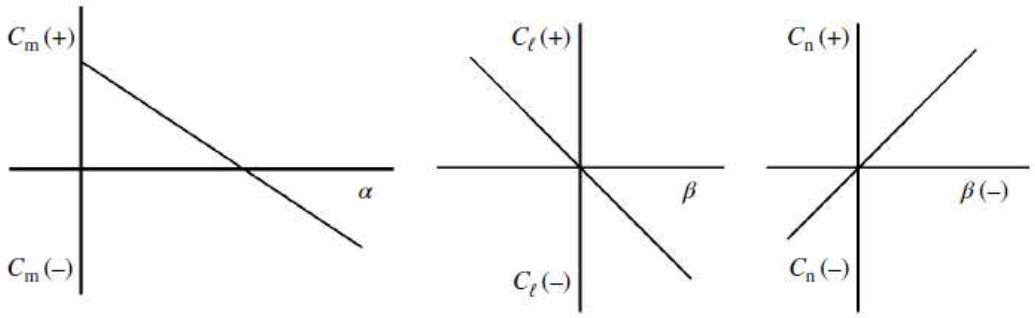

Figure 1.2 Stability conditions in pitch, roll and yaw.

2. Vortex Lattice Method

The vortex lattice method is a computational fluid dynamics method that provides data on complex problems by solving equations that control fluid dynamics and is reliable in a wide range of conditions to estimate aerodynamic load distribution and thus forces and momentum acting on the aircraft in the preliminary stages of aircraft design. The method operates on the foundation of an incompressible, inviscid and irrotational flow field, which is accurately represented by Laplace's equation. Furthermore, we assume a small angle of attack, as well as sideslip and that the lifting surface is thin, resulting in a neglected effect of thickness on aerodynamic forces.

2.1 Theoretical Background

As previously said, the flow is irrotational, which means that the vorticity is null at every point.

$$\xi = \nabla \times V = 0 \tag{2.1}$$

Defining φ as a scalar function, we get:

$$\nabla \times (\nabla \varphi) = 0 \tag{2.2}$$

Combining the previous two formulas:

$$V = \nabla \varphi \tag{2.3}$$

Which asserts that for an irrotational flow, there exists a scalar function φ such that the velocity is determined by the gradient of said function, hence the term velocity potential.

Applying the mass conservation principle for an incompressible flow:

$$\nabla \cdot V = 0 \tag{2.4}$$

Having previously defined the velocity potential, integrating (2.3) and (2.4):

$$\nabla \cdot (\nabla \varphi) = 0 \tag{2.5}$$

Or

$$\nabla^2 \varphi = 0$$

Namely the Prandtl-Glauert equation, which governs this irrotational and incompressible flow. Because irrotational and incompressible flow is a complicated flow pattern, its solution can be synthesized by adding up a number of elementary irrotational and incompressible flows.

2.1.1 Boundary Conditions

The vortex lattice method employs the linearization and transfer of the boundary condition, in addition to the linear approximation of velocity and pressure, known as the thin airfoil boundary condition. This allows for the influence of thickness and viscosity to be neglected.

The significance of this analysis is that the cambered surface boundary conditions could even be applied on a flat coordinate surface, resulting in a much easier approach for implementing the boundary conditions. Once applied to the Laplace's equation, considering a symmetrical airfoil, the camber effect can also be disregarded, and the problem can be simply solved by considering the effect of angle of attack on a flat surface. This is the working principle VLM employs.

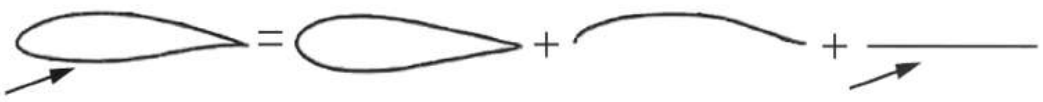

Figure 2.1 Working principle used by the VLM.

Considering a wing, on the x-y plane, according to the boundary conditions, the normal flow across the thin wing's solid surface is zero.

$$\nabla(\varphi + \varphi_\infty) = 0 \tag{2.6}$$

Which implies that the sum of the normal velocity components induced by the wing's bound vortices w_b, the wake w_i, and the free-stream velocity V will be zero.

$$w_b + w_i + V_\infty \cdot \alpha = 0 \tag{2.7}$$

2.1.2 Biot-Savart Law

One of the possible solutions to Laplace's equation is the two-dimensional vortex singularity. The flow induced by this filament is outlined by the Biot-Savart law:

$$dV_p = \frac{\Gamma}{4\pi} \cdot \frac{dl \times r_p}{|r_p|^2} \tag{2.8}$$

The induced velocity dV_p at a point P, due to a segment of a vortex filament dl a point q is directly proportional to the vortex strength Γ (which has the same sign as the vorticity, positive if clockwise) and inversely proportional to the square of the distance r_p.

The concept of a point vortex can be extended to the case of a general three-dimensional vortex filament, its induced flow field is shown in figure (2.2). We then obtain the induced velocity by integrating along the entire length of the vortex filament.

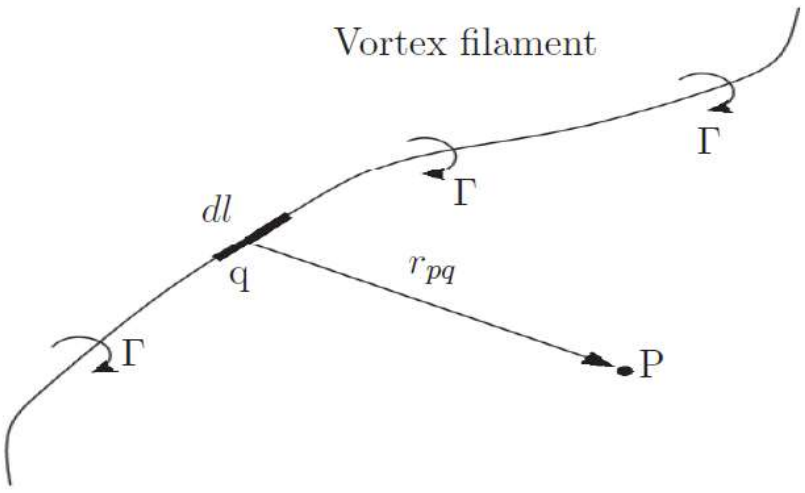

Figure 2.2 Flow induced by vortex filament.

2.1.3 Horseshoe Vortex

The VLM uses a specific type of vortex, known as the horseshoe vortex. The vortex line is assumed to be in the x-y plane in the scenario. It is made up of four vortex filaments: two trailing vortex segments AB and CD that begin in infinity and run parallel to the free stream, two finite vortex segments BC and AD.

Generally, due to the indefinite distance, the effects of AD are ignored; the horseshoe vortex has essentially three sections. The lifting properties are represented by the straight bound vortex segment BC, while the wake is represented by the two semi-infinite trailing vortex lines. The induced velocity at a point can be determined in general terms using the Biot-Savart law:

$$\mathrm{V}_p = \mathrm{V}_{bc} + \mathrm{V}_{b\infty} + \mathrm{V}_{c\infty} \tag{2.10}$$

It is necessary to evaluate V_p in order to obtain the location of P (control point) and the vortex in accordance with the surface boundary condition. A new equation for circulation can be then obtained by equating the lift equations from thin airfoil theory and the Kutta-Jukowski theorem. The bound vortex and control point positions are then determined by substituting the revised circulation equation to the boundary condition, which requires the induced velocity at the control point and the velocity at the boundary to be equal.

The "¼-¾ rule" indicates that the vortex is places at the ¼ chord point and the control point at the ¾ chord point. However, this is not a theoretical law; it is simply a substitution that works fairly well and has become a standard practice.

The model's surface is divided into a finite number of panels (chordwise and spanwise) on each of which there is a horseshoe vortex. Because each vortex has its own circulation, the overall aerodynamic force must be calculated by summarizing the contributions of all panels.

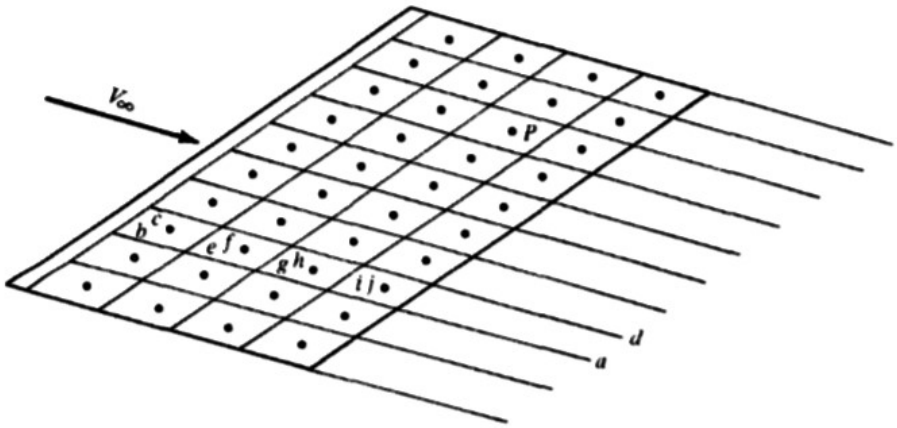

Figure 2.3 Lattice of horseshoe vortices.

2.1.4 Implementation in VSPAERO

The VLM is an extension of Prandtl's lifting line theory, with the crucial advantage of being able to deal with swept wings. With this method, the wing of an aircraft is modelled as a lattice of horseshoe vortices, rather than only one horseshoe vortex per wing, as in the lifting theory.

The VLM models the lifting surfaces as an infinitely thin sheet of discrete vortices to compute the lift curve slope, generated drag, and force distribution. It is essential to note that at this level, it is not possible to evaluate the viscous drag, however it is acceptable to compute the induced drag beginning with the production of lift. Because the VLM is based on potential flow theory, it is only valid in the linear aerodynamic region and thus only in the low angle of attack flight domain.

The horseshoe vortex's strength is calculated with the knowledge that the vector sum of vortex induced velocity and freestream contribution at each control point satisfies the boundary condition of a zero normal velocity component. In fact, having imposed the boundary condition, the only unknown term is Γ in the induced velocity formula. Once computed, it can be utilized in the Kutta-Jukowski theorem to evaluate load distribution and then lift. These values can also be used to calculate induced drag and momentum coefficients.

In its formal definition, VSPAERO does not use the VLM exactly but instead employs a mean surface technique. This indicates that the analysis takes into account the camber effects of wings and fuselages rather than thickness. Wings have the same camber as the chosen airfoil,

whilst fuselages are replaced by two mean surfaces arranged in a cross. Thus, on the wing surface we have a juxtaposition of a finite number of ring vortices of varying intensities, as this tool itself is a ring vortex-based solver.

3. Geometric Modelling

3.1 OpenVSP

Open Vehicle Sketchpad (OpenVSP) is an open-source parametric aircraft geometry, originally developed by Dave Kinney at NASA Ames. It enables the user to build three-dimensional models of aircrafts from common engineering parameters and the models obtained can be then processed in formats suitable for structural or aerodynamic analysis. The website can be accessed via the following link: http://openvsp.org

Upon launch, Open VSP displays a working window as well as a Geometry browser (Figure), the latter can be used to add all the individual components that make up an airplane. It also provides multiple basic aircraft geometry shapes, that can be altered utilizing the component geometry window, and can easily combined into an aircraft model.

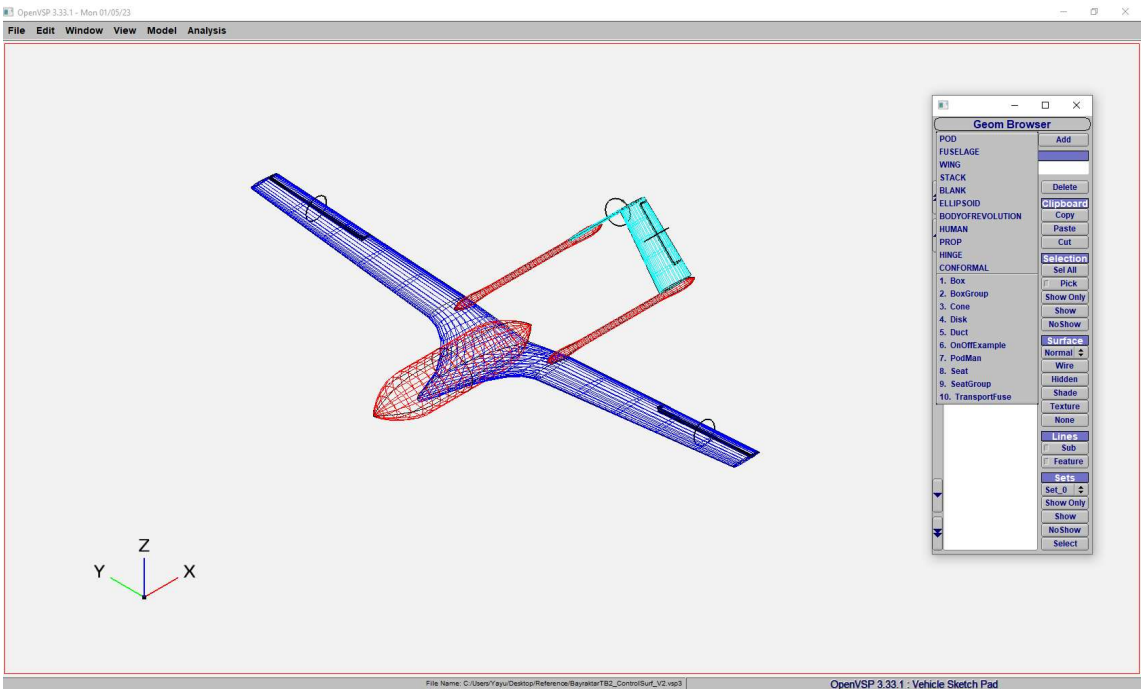

Figure 3.1 OpenVSP working window and geometry browser.

3.1.1 VSPAERO

VSPAERO is a tool provided by OpenVSP; it is a thin-surface code for inviscid subsonic and supersonic aerodynamics. It incorporates a single actuator disk model to depict the interaction of propulsion and aircraft, as well as the ability to calculate common stability derivatives.

VSPAERO fails to simulate stall or separation characteristics as it is a linear solver. It has integrated actuator disks that can be precisely specified for rapid and straightforward aero-propulsive study. It includes a Viewer tool that displays wakes and the change in pressure coefficient.

The control grouping VSPAERO GUI tab facilitates the construction of groups of control surfaces in the VSPAERO configuration file. All rectangular surfaces and control subsurfaces that can be added to a group are listed in the Available Control Surfaces browser. Subsurface gains can be altered to allow control surfaces within a group to be mixed.

The VSPAERO's vortex lattice solver requires the degenerate geometry file, a three-dimensional model representation in progressively simpler frames. First the entire three-dimensional model is represented, followed by a plane representation, and then by a stick representation.

In order to start the analysis, operational conditions must be defined. The provided drag output only contains information about the induced drag. Using components in the DegenGeom build file that do not affect lift, such as the nacelle and fuselage, may result in increased operating time with no valuable return. When utilizing this tool, the lift surfaces, such as the wing and horizontal stabilizer, are the major components that control the output values. These files can be opened with software such as Notepad or Excel.

Although the minor impact other components have on the vehicle's aerodynamic drag, the generated drag determined by VSPAERO is mostly based on the lift coefficient.
When running the vortex lattice method, VSPAERO will generate a number of files containing critical information for model analysis.
The software collects the data in text files to be then elaborated in Excel. The files used in this work are POLAR files for global aircraft's coefficients and finally STAB files for control and stability derivatives.

3.2 Bayraktar modelling

In this chapter we briefly illustrate how the model has been constructed with the tools above mentioned, from the basic wing geometry to the fuselage and the tailplane as well as the control surfaces.

Figure depicts the reference utilized to realize this model.

The measurements not shown in the design were approximated using Adobe Acrobat Reader's measuring tool and expressed in feet on OpenVSP.

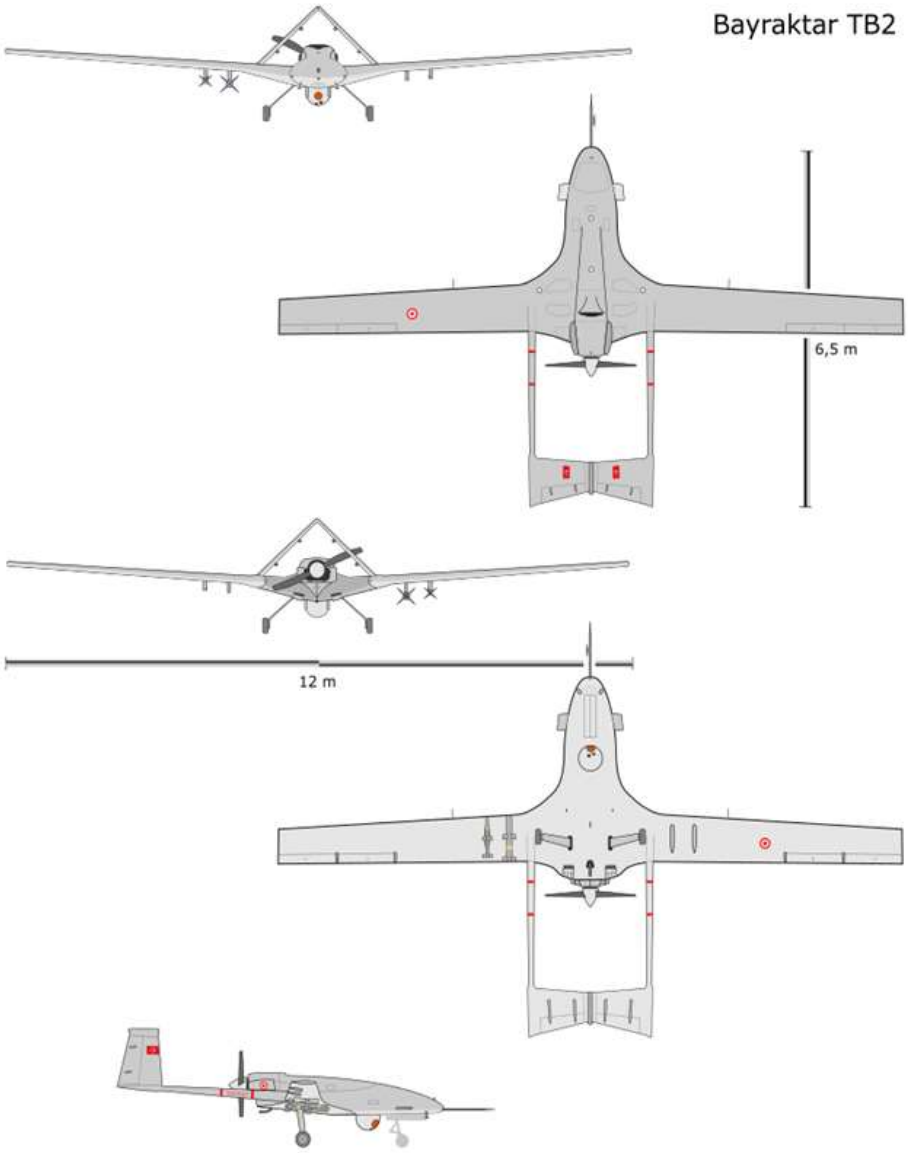

Figure 3.2 Bayraktar TB-2 reference.

3.2.1 Wing

The wing of the UAV has been designed as follows:

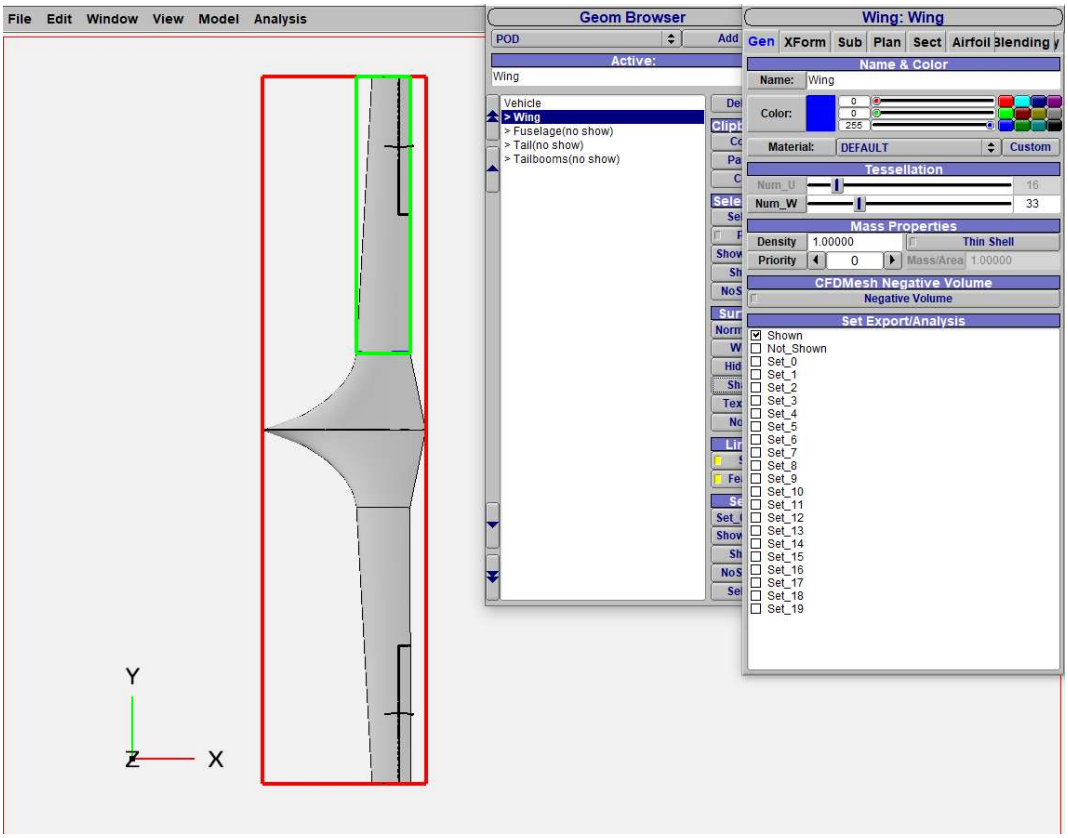

Figure 3.3 Wing ad wing geometry window

The wing has been split into two sections, each of which is distinguished by an airfoil based on whether it is root, kink, or tip. Since the wing section is unknown, by visual inspection of some photographs of the aircraft we assumed the NACA 2415 airfoil for root and kink profiles, and NACA 1412 airfoil for the tip. Their parameters and performance have been obtained from the website www.airfoiltools.com.

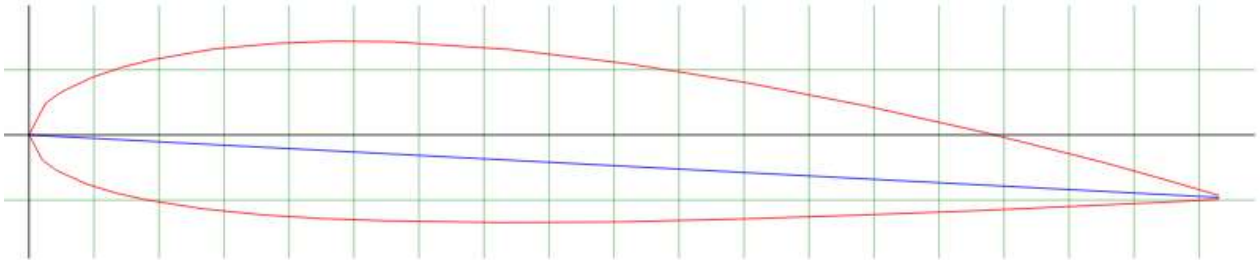

Figure 3.4 Root and kink airfoil profile (NACA 2415).

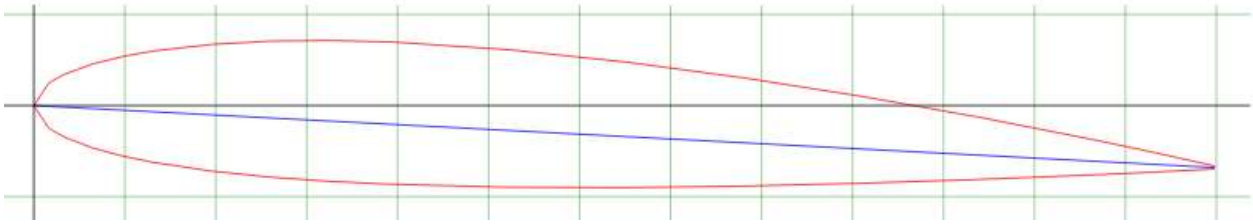

Figure 3.5 Tip airfoil profile (NACA 1412).

3.2.1 Wing Grid Refinements

We now begin this paragraph with an assessment of the wing grid by adjusting the grid chordwise and spanwise. In both situations, the desired outcome is to obtain a pair of values U and W such that the polar curves derived from altering one of said parameters, while maintaining the other constant, reach an asymptotic trend, at a fixed angle of attack.

The first step is to adjust the grid chordwise by varying the W value using the tools made available in the wing geometry tab. To proceed with this first evaluation the U value has been set to the default setting of 16, and the angle of attack to 0°. As it can be seen from the tables below, after a specific number of sections, the coefficients CL, CD and CM remain fairly stable as W is increased further. We may conclude that the value of W=77 will suffice for the following studies.

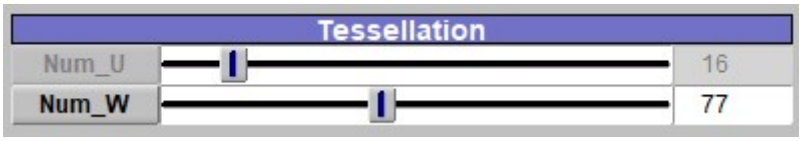

Figure 3.6 Tessellation adjustment bar.

Considering the prior premise, the transverse direction refinement was accomplished by altering the U parameter in the wing geometry window Sect Tab, assuming now as fixed the previously found value of W. Observing the Oswald efficiency factor after completing this study reveals the asymptotic trend. This behaviour is clearly more noticeable with the spanwise refinement; in addition, raising the value of the parameter U has an incredibly high influence on the solution time, therefore causing an increase of the computational cost. We may also take note of the fact that the wing model is made up of two sections, ergo the number of slices must be proportionally distributed between the two.

The pair of W and U values that are essential for building the grid are therefore W=77 and U=40. The same grid will be used for the tailplane, keeping in mind that the priority of this

study is to focus on the aircraft's load-bearing surfaces in order to be consistent with how OpenVSP operates.

3.2.2 Fuselage

The fuselage, like any other geometric component, has a geometric modelling window, which allows to enter the main measurements.

It was possible to rebuild the curvature of the fuselage section by section by altering the parameter Z by displaying the design reference as a background to the design window.

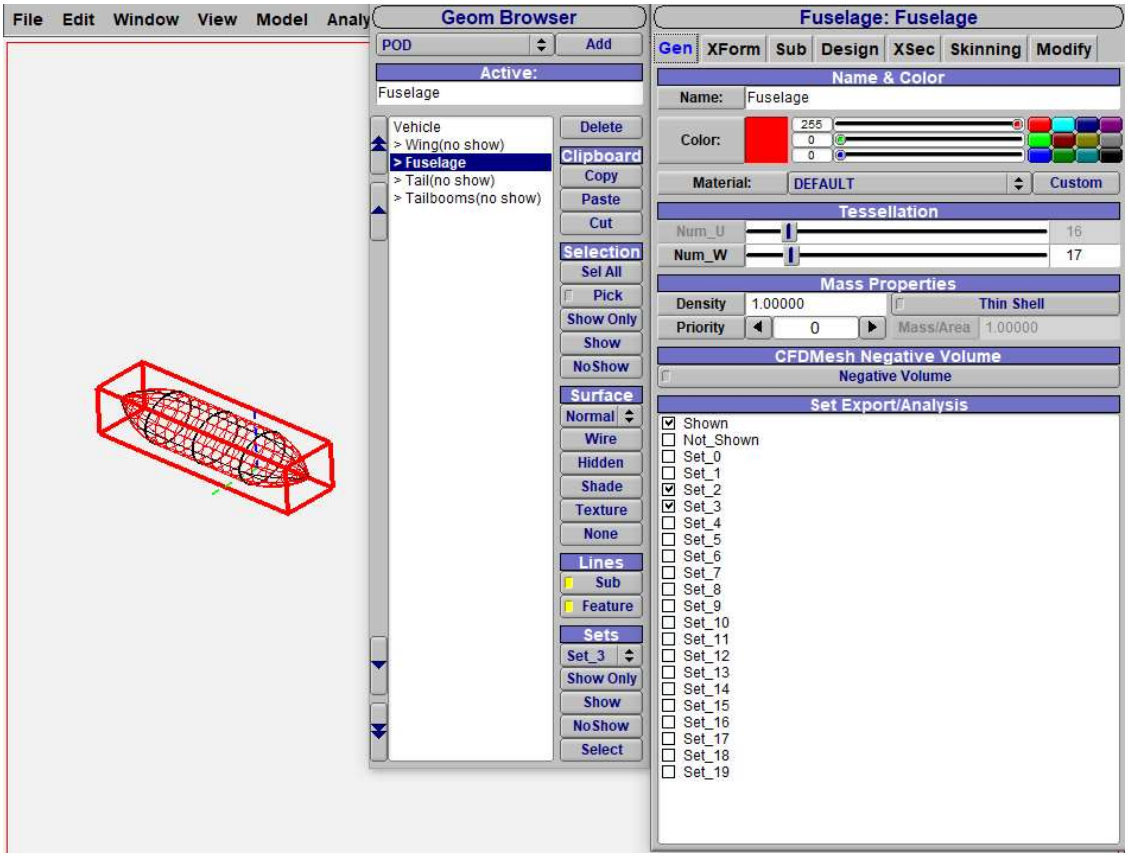

Figure 3.7 Fuselage geometry window.

3.2.3 Tailplane

The Horizontal Tail basic geometric parameters need to be entered in the design window, using the same grid that was used for the wing was also used for the horizontal tail. NACA 0010 airfoil was chosen as the profile.

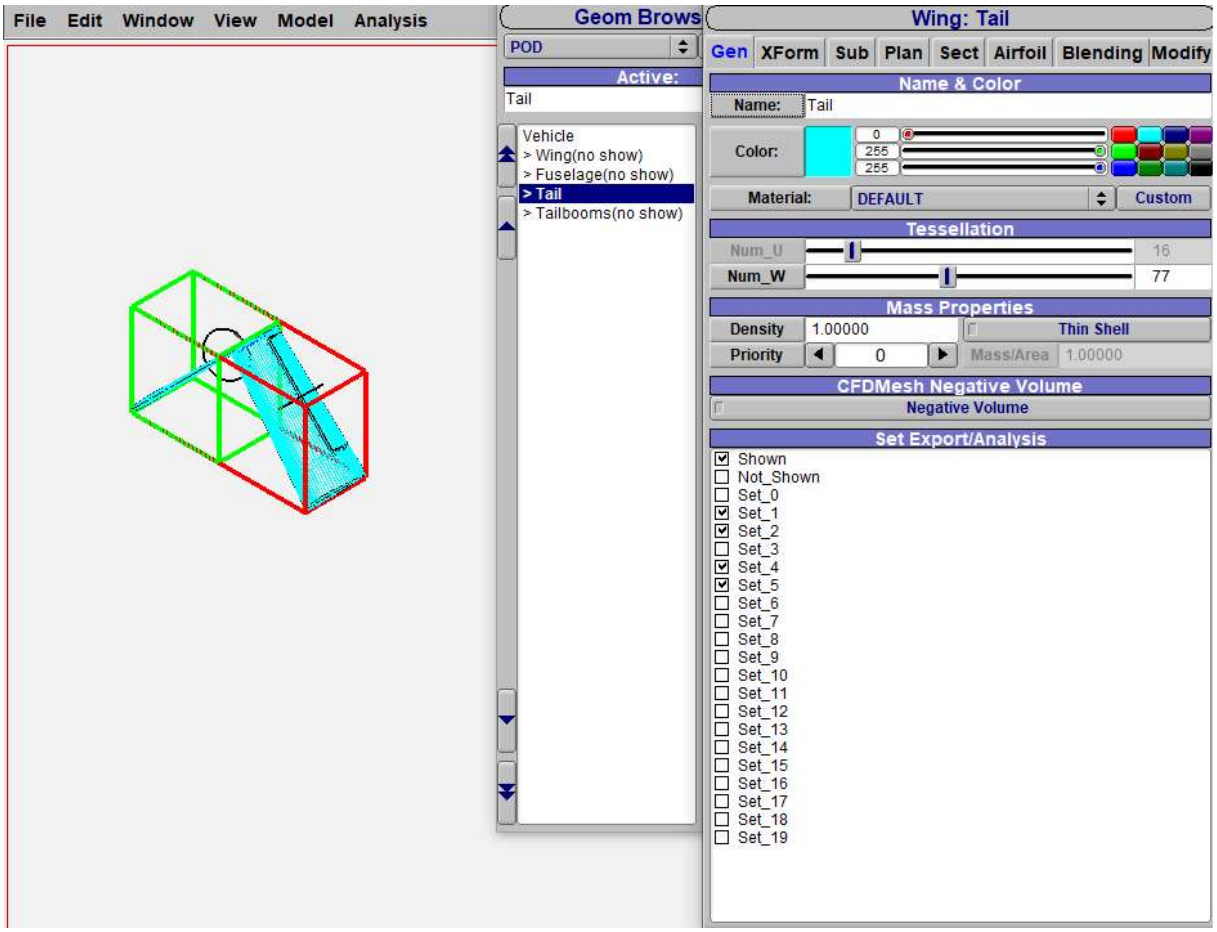

Figure 3.8 Tailplane geometry window.

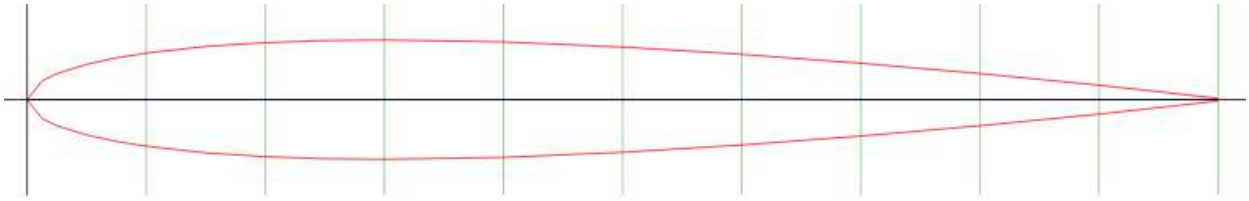

Figure 3.9 Tailplane airfoil profile *(*NACA 0010).

The booms have been modelled as slender fuselages. Due to the XZ plane symmetry, only one of the two boom parameters is shown.

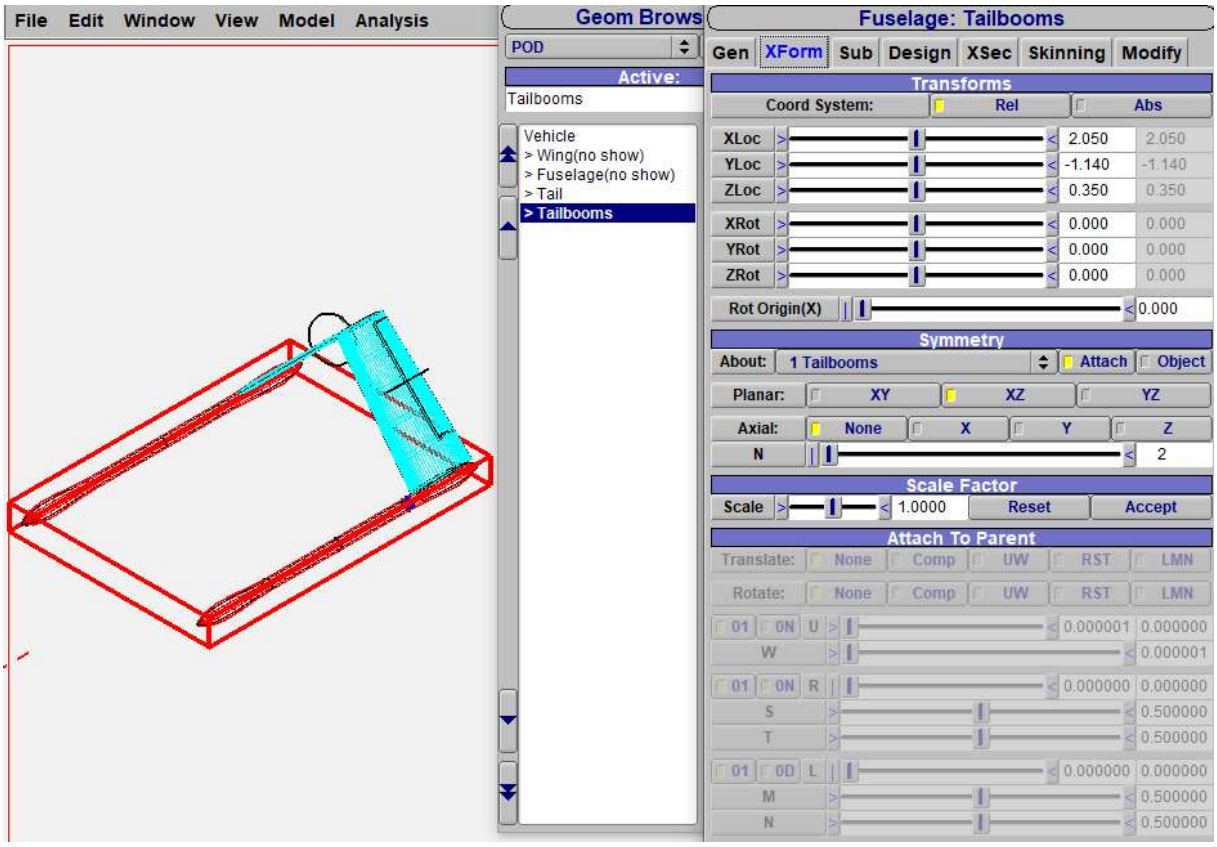

Figure 3.10 Tailbooms geometry window.

4. Results and longitudinal aerodynamic analysis

As previously stated, the study was carried out using the VSPAERO module and the Vortex Lattice (VLM). The user can select moment reference location and reference dimensions, or let the tool evaluate these quantities from the model.

References Area and lengths have been estimated from the model. The Flow Conditions were changed to have six Alpha Start values ranging from 0° to 10°, Beta Start permanently null, Mach fixed at 0.1, and Reynolds number fixed at 2e+06 according to Bayraktar cruise speed, and CG as moment reference position, which was obtained by VSPAERO.

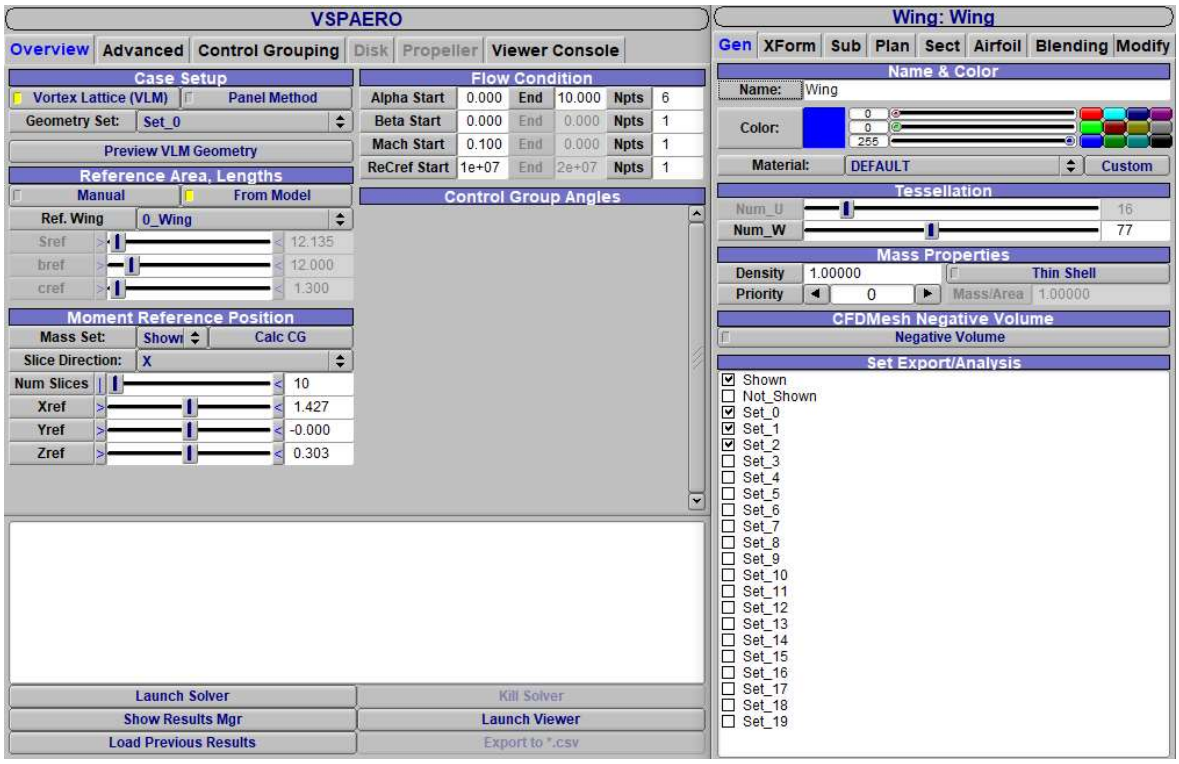

Figure 4.1 VSPAERO and set selection panels.

Once the geometry of the airplane has been determined, we may proceed with the aerodynamic analysis of the contribution of each component, which can be done by selecting the desired set in the VSPAERO analysis panel.

All the subsequent calculations were carried out with the wing geometry fixed and the wing grid set up as previously mentioned, while control surfaces have been disabled.

4.1 Aerodynamic curves

This paragraph compares the 3D aerodynamic curves of an isolated wing (W), of the wing and tail combination (WT), and then of the entire aircraft including tail booms, as they have a negligible effect on the quantities analysed.

α	C_{L_W}	$C_{L_{WT}}$	C_L
0°	0.234	0.212	0.233
2°	0.395	0.380	0.398

4°	0.555	0.547	0.559
6°	0.716	0.710	0.710
8°	0.875	0.869	0.885
10°	1.033	1.053	1.065

Table 4.1 Lift coefficients for the wing, wing and tail, complete aircraft.

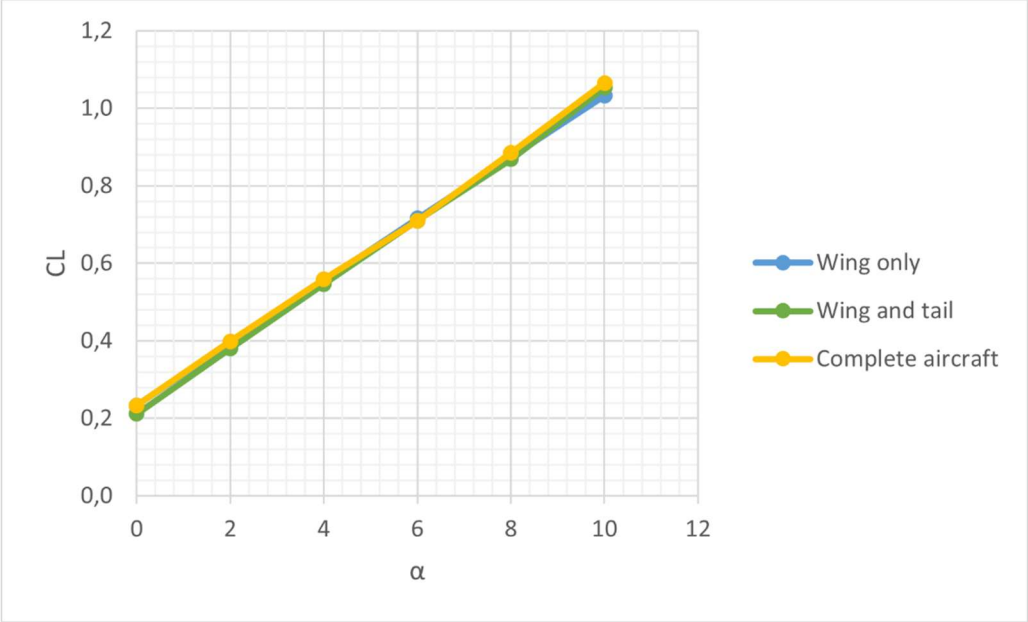

Figure 4.2 Lift coefficient curves for the three sets of components

Because VSPAERO cannot execute stall conditions, the graph in Figure 4.2 only depicts the linear segment of a true lift coefficient curve.

It is clear that the fuselage and tail booms have little impact on the wing's lift properties and that the linear behaviour is conserved in all situations examined, while the addition of Horizontal Tail and fuselage raises the slope of the C_{L_α} curve, as the added surface is load-bearing, but the reference area to normalize the coefficient remains the wing planform area S.

α	C_{M_W}	$C_{M_{WT}}$	C_M
0°	-0.012	0.037	0.046
2°	-0.006	0.028	0.039
4°	-0.001	0.022	0.036
6°	0.003	0.013	0.029
8°	0.007	-0.013	-0.012
10°	0.010	-0.051	-0.025

Table 4.2 Pitching moment coefficients for the wing, wing and tail, complete aircraft.

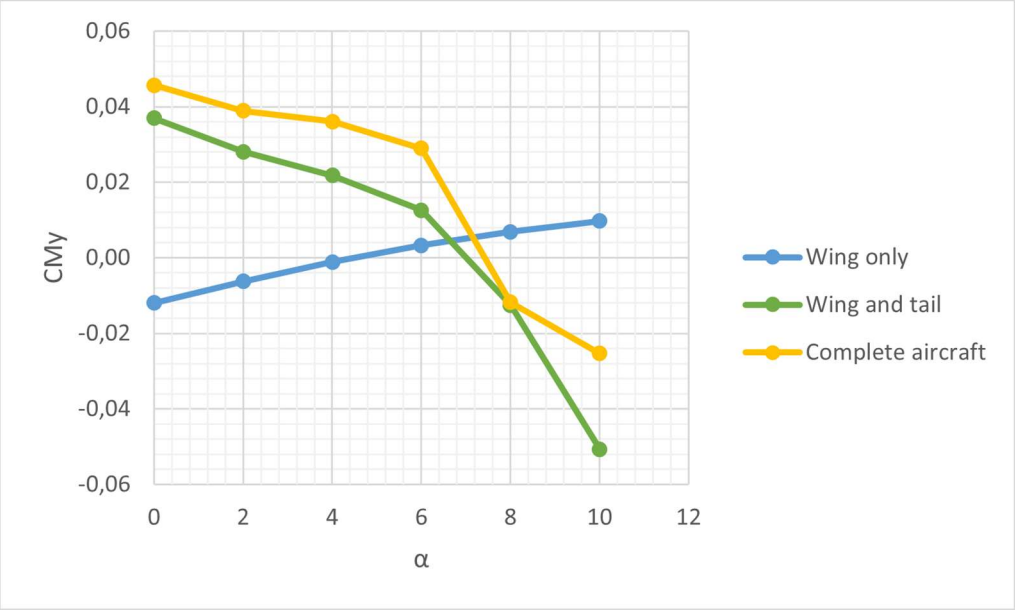

Figure 4.3 Pitching moment coefficient curves.

To compute the pitching moment, the CG has been positioned at 75% of the fuselage length. Looking at Table 4.2 and Figure 4.3, for the pitching moment, it is apparent that the isolated wing exhibits a stable behaviour just as the wing body and the Bayraktar in its entirety. The UAV in question is longitudinally stable with a negative CMα slope through the equilibrium point.

The change in pitching moment slope for the wing alone and wing-tail combination can be traced back to the wake impacting on the inverted V tailplane.

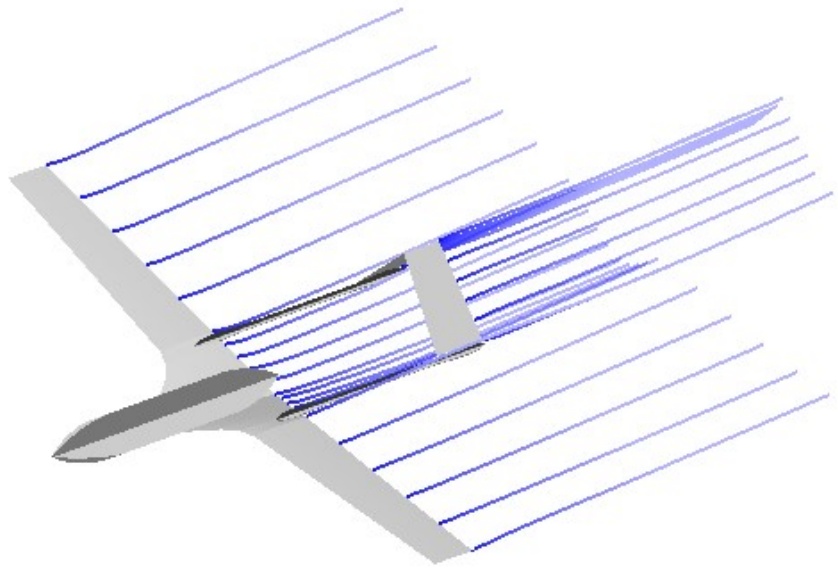

Figure 4.4 Trailing wakes at α=4°

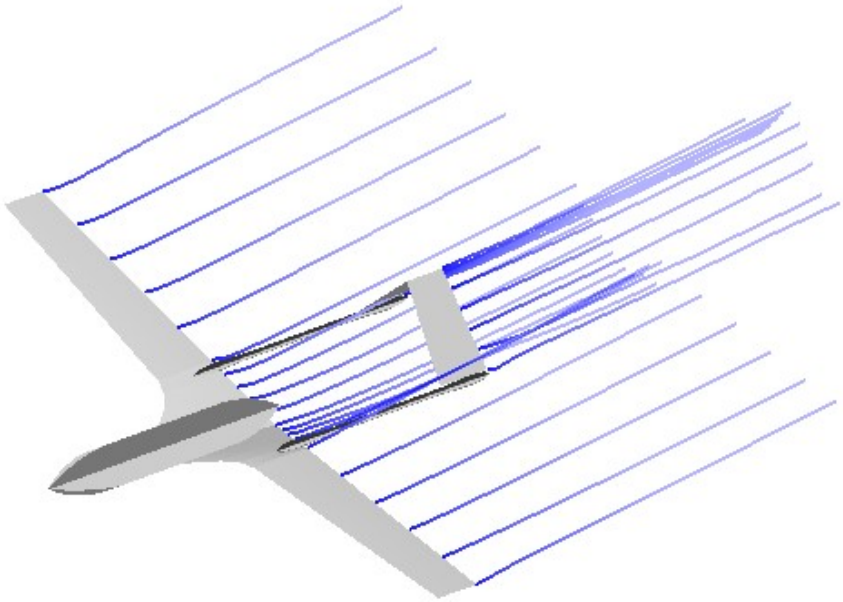

Figure 4.5 Trailing wakes at α=8°

Using the data from the previous tables and the Excel SLOPE function, we can estimate useful derivatives for the three configurations. We can obtain $C_{L\alpha}$, which is the total aircraft's lift curve slope

$$C_{L_\alpha} = 0.0825 \text{ deg}^{-1} \quad (4.1)$$

As well as $C_{M\alpha}$ that is the total aircraft's pitching moment curve slope, which is negative, as expected from the table

$$C_{M_\alpha} = -0.0073 \text{ deg}^{-1} \tag{4.2}$$

The addition of the fuselage leads the CL/CD efficiency curve to shift to lower values when the angle of attack reaches 8°, owing to the increased parasite drag and hence the CD.

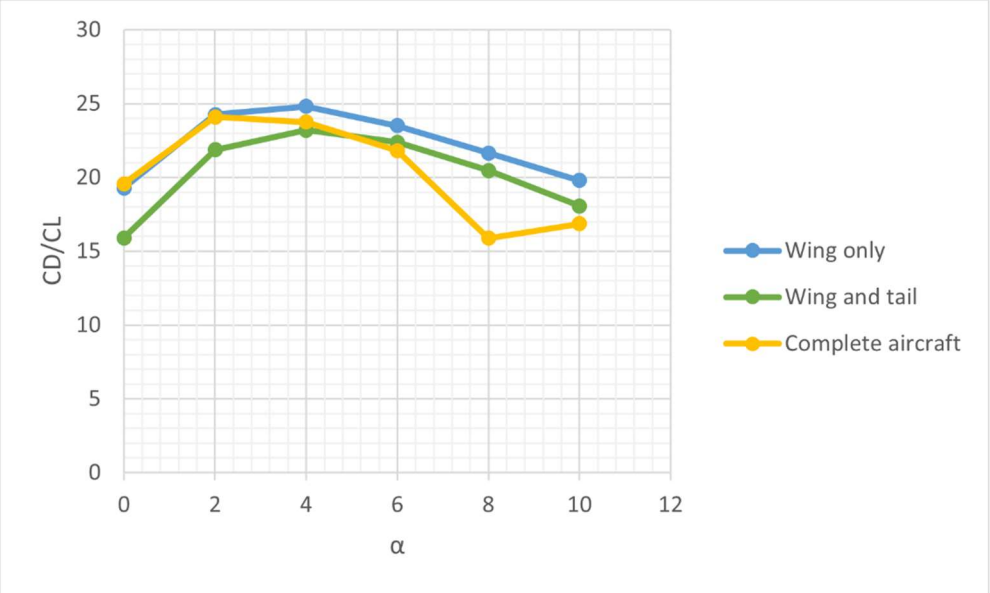

Figure 4.6 Aerodynamic efficiency curves.

α	C_{D_W}	$C_{D_{WB}}$	C_D
0°	0.012	0.013	0.012
2°	0.016	0.017	0.017
4°	0.022	0.024	0.024
6°	0.031	0.032	0.033
8°	0.040	0.043	0.056
10°	0.052	0.058	0.063

Table 4.3 Drag coefficients for the wing, wing body and complete aircraft.

It is apparent the minimal effect of fuselage on drag, and this is due to the way VSPAERO computes drag. In reality, the tool solely calculates induced drag, so only lifting surfaces contribute to the curve.

4.2 Neutral Point

To determine the neutral stability condition, the neutral point must be calculated. The first step is to linearize the aircraft pitching moment coefficient and set the equation linked to $C_{M\alpha}$ to zero:

$$C_{M_\alpha} = C_{L_{\alpha,W}} \cdot (\overline{XG} - \overline{X}_{ac,WB}) - \eta_H \frac{S_H}{S} (\overline{X}_{ac,H} - \overline{XG}) C_{L_{\alpha,H}} \left[1 - \left(\frac{d\epsilon}{d\alpha}\right)_H\right] = 0 \tag{4.3}$$

At this point, the neutral point extended expression can be extracted by noting that when $\overline{XG} = \overline{XN}$, the airplane's pitch equilibrium is neutrally stable and assuming $C_{L_{\alpha,WB}} = C_{L_{\alpha,W}}$:

$$\overline{XN} \equiv \frac{XN}{\bar{c}} = \frac{\bar{X}_{ac,WB} + \eta_H \frac{C_{L_{\alpha,H}} S_H \bar{X}_{ac,WB} \left[1 - \left(\frac{d\epsilon}{d\alpha}\right)_H\right]}{C_{L_{\alpha,WB}} S}}{1 + \eta_H \frac{C_{L_{\alpha,H}} S_H \left[1 - \left(\frac{d\epsilon}{d\alpha}\right)_H\right]}{C_{L_{\alpha,WB}} S}} \tag{4.4}$$

The concept of static stability margin can be defined using the neutral point:

$$SM = \overline{XG} - \overline{XN} \tag{4.5}$$

Another valuable formulation for C_{M_α} comes from the following equation:

$$C_{M_\alpha} = C_{L_\alpha}(\overline{XG} - \overline{XN}) = C_{L_\alpha} SM \tag{4.6}$$

Therefore, in order to have a stable aircraft, $\overline{XG} < \overline{XN}$ specifically, $C_{M_\alpha} < 0$ and $SM < 0$ (typically $\approx 0.10 \div 0.20$)

Considering the horizontal tail volume ratio, defined as follows and independent from the CG location:

$$\overline{v_H} = \frac{S_H}{S} \frac{l_H}{\bar{c}} = \frac{S_H}{S} \left(\bar{X}_{ac,H} - \overline{XG}\right) \tag{4.7}$$

A new simplified expression for the neutral point can be obtained:

$$\overline{XN} \approx \bar{X}_{ac,WB} + \eta_H \frac{C_{L_{\alpha,H}}}{C_{L_{\alpha,WB}}} \overline{v_H} \left[1 - \left(\frac{d\epsilon}{d\alpha}\right)_H\right] \tag{4.8}$$

Knowing this we can calculate the neutral point:

$$\mathrm{XN} = 1.927\ \mathrm{m} \tag{4.9}$$

As well as the static margin:

$$\mathrm{SM} = -0.068 \tag{4.10}$$

4.3 Ruddervators effect on aerodynamic curves

The primary objective of this analysis is to highlight the impacts of the ruddervators deflection on the aerodynamic curves previously displayed. The analyses were carried out with both symmetric and antisymmetric deflection as to show the consequences of both configurations and how they influence both pitching moments and longitudinal stability.

The Control Group Angles panel (Figure 4.5) was used to change the subsurfaces deflection while keeping the control surfaces all at 0°; in fact, the angles chosen for the deflections were 0°, 15°, and 30°. The results of the analysis derived from the inputs entered in the panel are displayed using summary tables and graphs, both for symmetric and antisymmetric deflections.

Figure 4.7 Control group window.

Because VSPAERO's settings are diametrically opposed directions of rotation in the moving surfaces of the tailplane, we assume the -1 the Deflection Gain per Surface for one of the

ruddervators, such that a positive rotation corresponds to a downward deflection of both subsurfaces, as seen in Figure 4.6.

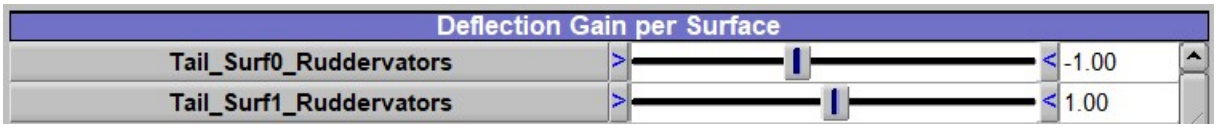

Figure 4.8 Deflection gain bar.

Now the results of the analysis will be presented.

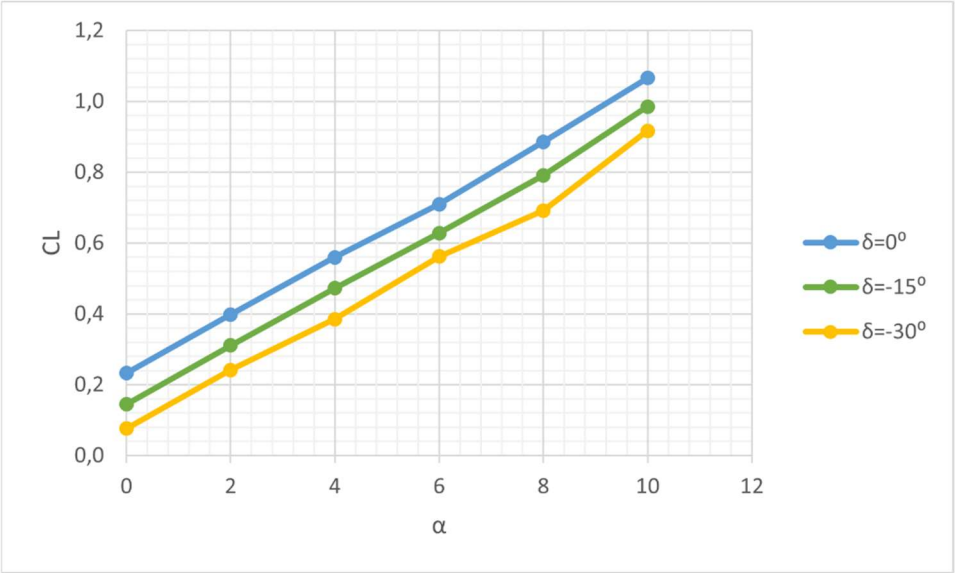

Figure 4.9 Lift coefficient curves with different symmetric rudder deflections

Symmetric ruddervator deflections imply stronger downforce on the tailplane and thus smaller global aircraft lift coefficients as clearly shown in Figure 4.5 and Table 4.4.

$\boldsymbol{\alpha}$	$\boldsymbol{C_L(\delta_e = 0°)}$	$\boldsymbol{C_L(\delta_e = -15°)}$	$\boldsymbol{C_L(\delta_e = -30°)}$
0°	0.233	0.145	0.076
2°	0.398	0.311	0.242
4°	0.559	0.472	0.385
6°	0.710	0.628	0.562
8°	0.885	0.791	0.692
10°	1.066	0.985	0.916

Table 4.4 Lift coefficients for symmetric deflections

Although the unique tailplane's design and control surfaces, antisymmetric ruddervator deflections (ruddervators utilized as rudders) do not affect the Bayraktar's lift generation, as shown in Table 4.4.

α	$C_L(\delta_e = 0°)$	$C_L(\delta_e = \pm 15°)$	$C_L(\delta_e = \pm 30°)$
0°	0.233	0.234	0.237
2°	0.398	0.393	0.387
4°	0.559	0.554	0.549
6°	0.710	0.709	0.704
8°	0.885	0.876	0.855
10°	1.066	1.065	1.058

Table 4.5 Lift coefficients for antisymmetric deflections

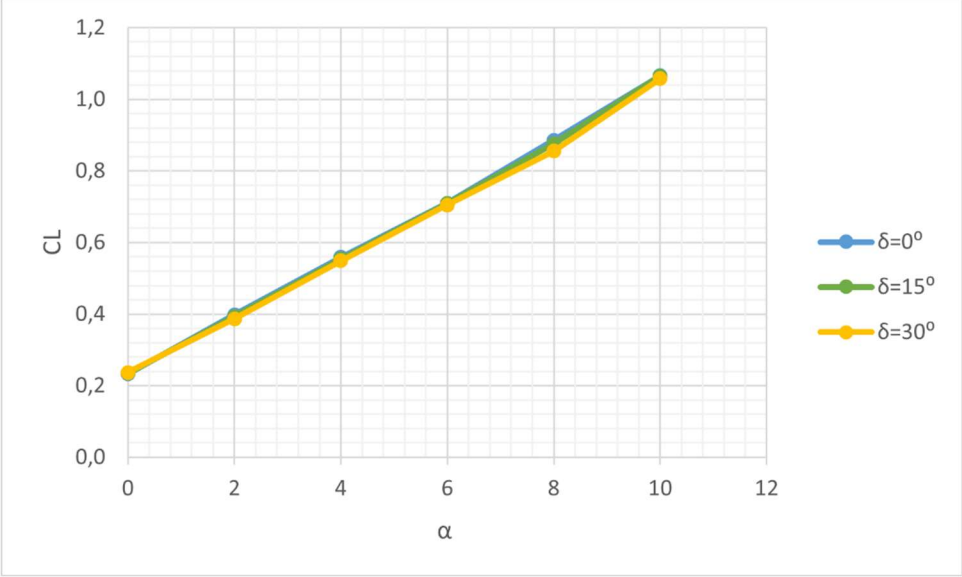

Figure 4.10 Lift coefficient curves with different antisymmetric rudder deflections

With the same process we can analyse data regarding the pitching moment coefficient, for the different deflections.

α	$C_M(\delta_e = 0°)$	$C_M(\delta_e = -15°)$	$C_M(\delta_e = -30°)$
0°	0.046	0.262	0.434
2°	0.039	0.252	0.425
4°	0.036	0.249	0.421
6°	0.029	0.245	0.422
8°	-0.012	0.213	0.403
10°	-0.025	0.191	0.367

Table 4.6 Pitching moment coefficients for symmetric deflections.

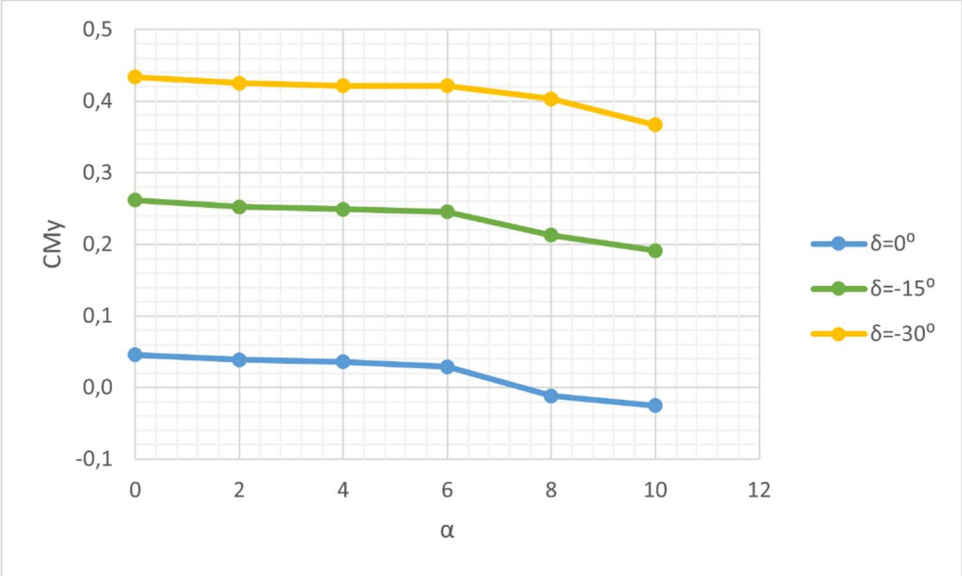

Figure 4.11 Pitching moment curves for symmetric deflections.

As with lift, let's investigate if antisymmetric ruddervator deflections affect the aircraft's pitching moment. It is obvious from the following data that ruddervators utilized as a rudder have no substantial effect on pitching moment.

α	$C_M(\delta_e = 0°)$	$C_M(\delta_e = \pm 15°)$	$C_M(\delta_e = \pm 30°)$
0°	0.046	0.045	0.044
2°	0.039	0.048	0.060
4°	0.036	0.044	0.059
6°	0.029	0.041	0.058
8°	-0.012	-0.002	-0.012
10°	-0.025	-0.015	0.003

Table 4.7 Pitching moment coefficients for antisymmetric deflections.

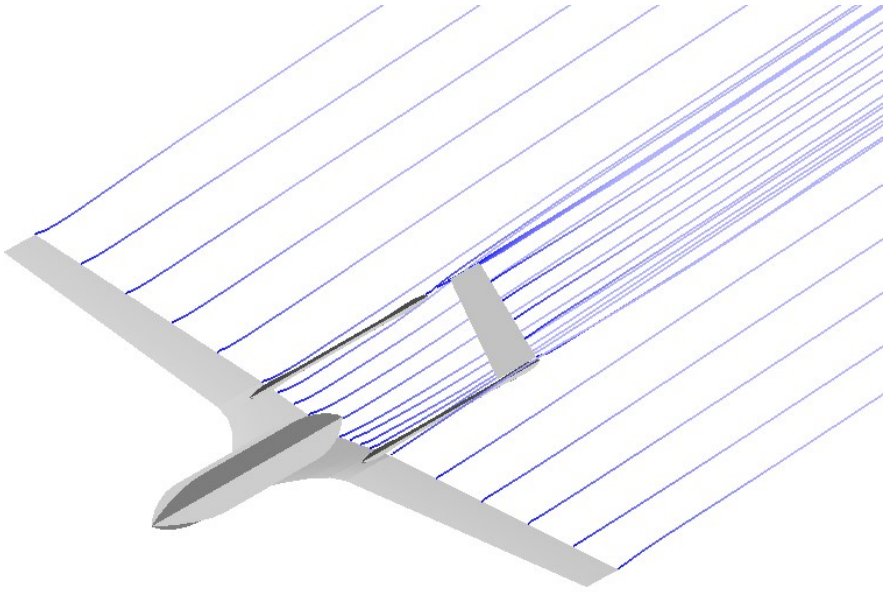

Figure 4.12 Wakes for δ=0°

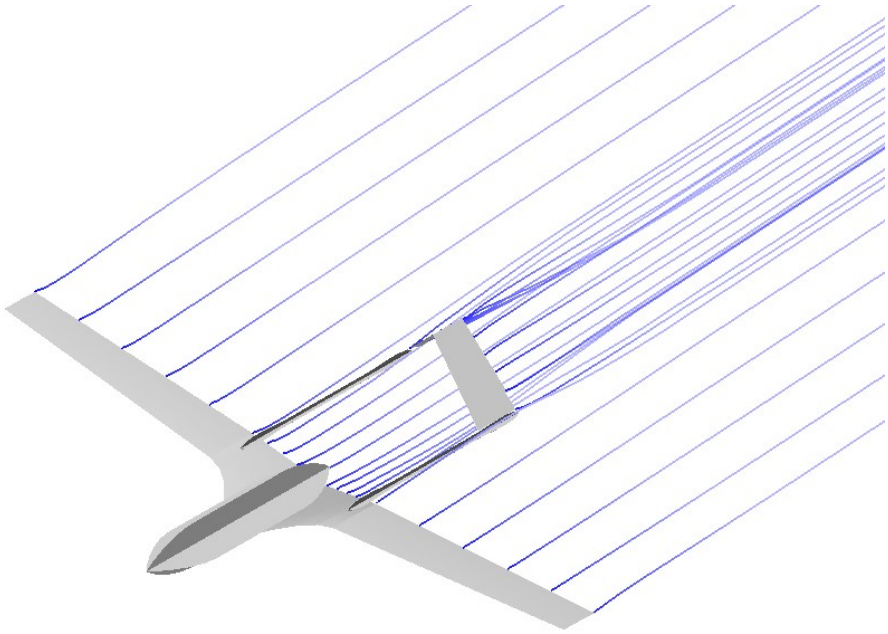

Figure 4.13 Wakes for δ=15°

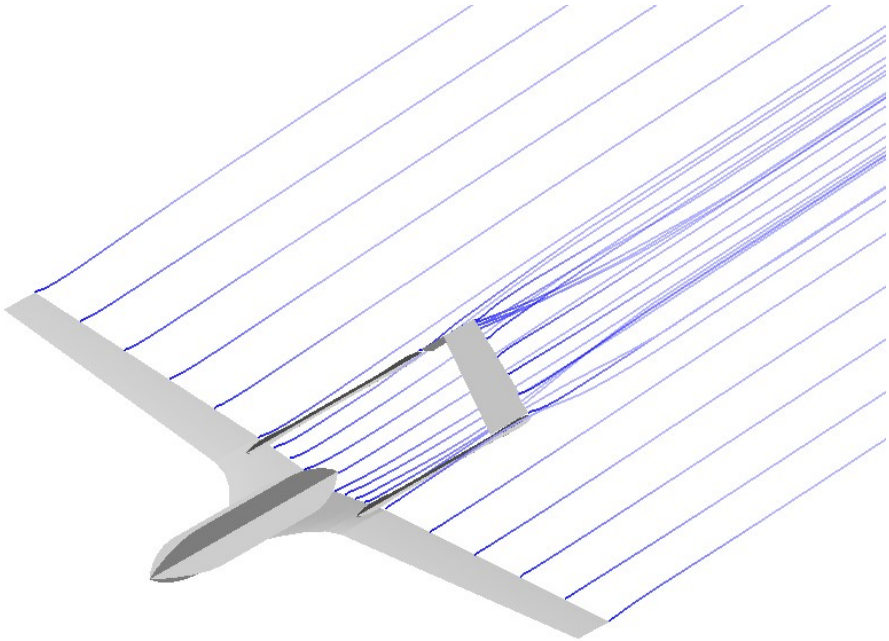

Figure 4.14 Wakes for δ=30°

Finally, the data obtained concerning the drag coefficient and aircraft efficiency for symmetric deflections is presented.

α	$C_D(\delta_e = 0°)$	$C_D(\delta_e = -15°)$	$C_D(\delta_e = -30°)$
0°	0.012	0.014	0.022
2°	0.017	0.017	0.023
4°	0.024	0.022	0.026
6°	0.033	0.029	0.032
8°	0.056	0.041	0.040
10°	0.063	0.058	0.058

Table 4.8 Drag coefficients for symmetric deflections.

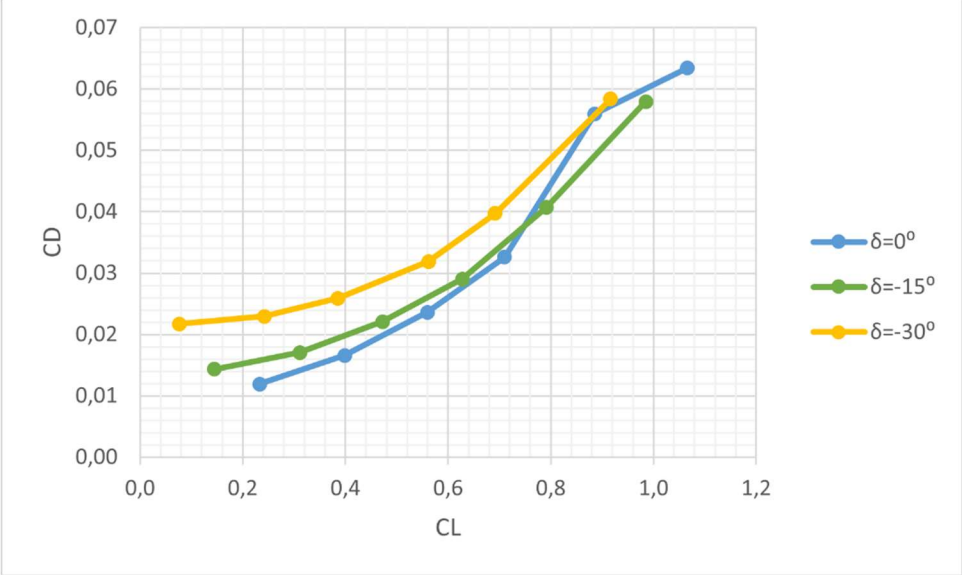

Figure 4.15 CD vs. CL curves for symmetric deflections.

α	$C_L/C_D(\delta = 0°)$	$C_L/C_D(\delta = -15°)$	$C_L/C_D(\delta = -30°)$
0°	19.58	10.09	3.52
2°	24.10	18.31	10.55
4°	23.76	21.42	14.91
6°	21.82	21.69	17.67
8°	15.87	19.50	17.47
10°	16.86	17.06	15.75

Table 4.9 CL/CD vs. alpha for symmetric deflections.

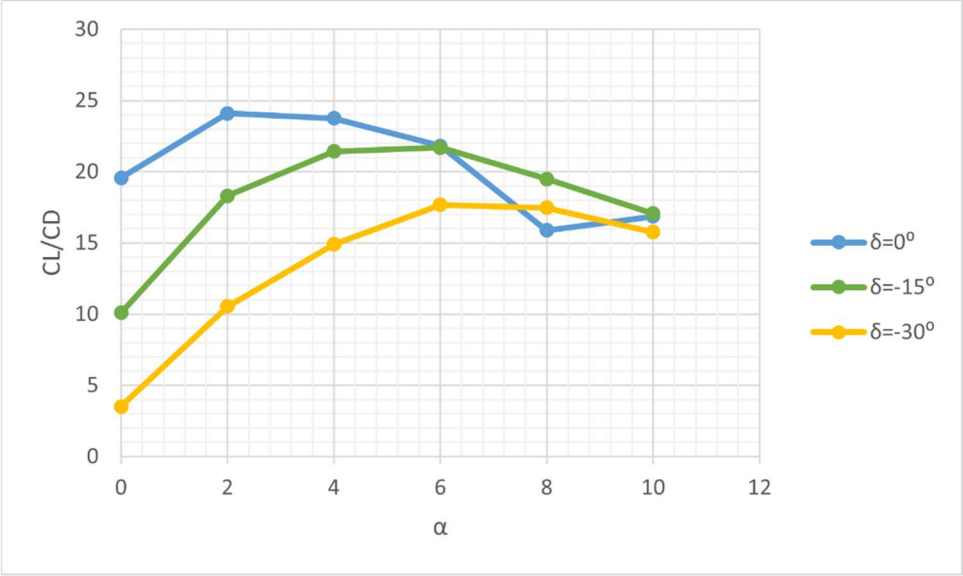

Figure 4.16 CL/CD vs. α curves

4.4 Longitudinal stability and control derivatives

To obtain the STAB file containing stability and control derivatives, we must select VSPAERO "steady stability" mode in the advanced panel and disable the XZ symmetry.

Figure 4.17 VSPAERO mode selection menu.

Starting with the data that was first entered, the VSPAERO stability module applies a delta of 1 degree to the angles. As a result, it represents a convenient tool to analyze an aircraft's stability characteristics, but it is deemed less accurate than linear regression applied to a wider set of data. The results are summarized in Table 4.19 only containing the derivatives we are interested in.

Derivative	Value
$C_{M_{x_\beta}}$	0.04768
$C_{M_{y_\alpha}}$	-0.11945
$C_{M_{z_\beta}}$	-0.04210
C_{L_α}	0.08324
$(C_{M_x})_{\text{antisym}}$	0.00016
$(C_{M_y})_{\text{antisym}}$	0.04544
$(C_{M_z})_{\text{antisym}}$	0.00094
$(C_{M_x})_{\text{sym}}$	0.00024
$(C_{M_y})_{\text{sym}}$	0.05966
$(C_{M_z})_{\text{sym}}$	0.00002

Table 4.10 Stability derivatives (in $\boldsymbol{deg^{-1}}$).

Note that the C_{L_α} derivative almost corresponds to the value that was previously estimated using the SLOPE function in Excel.

5. Conclusions

This thesis demonstrated how to perform a thorough aerodynamic analysis of an airplane using OpenVSP and VSPAERO which have demonstrated to have an outstanding design. As previously stated, VSPAERO is incapable of evaluating some aerodynamic phenomena; nonetheless, the goal of this software is not to produce completely reliable aerodynamic studies, but rather to make them quick and simple, bypassing the need for lengthy CFD simulations or wind tunnel experiments. That said, it undoubtedly has limitations for more sophisticated models, but it is a reasonable solution for simpler ones that require a preliminary numerical analysis to be compared with actual wind tunnel experiments.

Bibliography

[1] Advanced UAV aerodynamics, Flight stability and control, Pascual Marqués, Andrea Da Ronch John Wiley & Sons, Apr 27, 2017.

[2] Unmanned Aircraft Systems: UAVS Design, Development and Deployment, Reg Austin, John Wiley & Sons, Sep 20, 2011

[3] Software Testing: VSPAERO, Floris Mariën, Prof. Dr.-Ing. Dieter Scholtz, 16/07/2021

[4] OpenVSP website: http://openvsp.org

[5] Airfoil Tools website: http://airfoiltools.com